Electronic structure of $LiCoO_2$ thin films: A combined photoemission spectroscopy and density functional theory study

David Ensling,[1,2,*] Andreas Thissen,[1,3] Stefan Laubach,[4] Peter C. Schmidt,[4] and Wolfram Jaegermann[1]
[1]*Fachbereich Materialwissenschaften, Fachgebiet Oberflächenforschung, Technische Universität Darmstadt, Petersenstraße 23, D-64287 Darmstadt, Germany*
[2]*VARTA Microbattery GmbH, Daimlerstrasse 1, D-73479 Ellwangen, Germany*
[3]*SPECS GmbH, Voltastrasse 5, D-13355 Berlin, Germany*
[4]*Eduard-Zintl-Institut für Anorganische und Physikalische Chemie, Technische Universität Darmstadt, Petersenstraße 21, D-64287 Darmstadt, Germany*
(Received 6 December 2009; revised manuscript received 11 July 2010; published 16 November 2010)

The electronic properties of $LiCoO_2$ have been studied by theoretical band-structure calculations (using density functional theory) and experimental methods (photoemission). Synchrotron-induced photoelectron spectroscopy, resonant photoemission spectroscopy (ResPES), and soft x-ray absorption (XAS) have been applied to investigate the electronic structure of both occupied and unoccupied states. High-quality PES spectra were obtained from stoichiometric and highly crystalline $LiCoO_2$ thin films deposited "*in situ*" by rf magnetron sputtering. An experimental approach of separating oxygen- and cobalt-derived (final) states by ResPES in the valence-band region is presented. The procedure takes advantage of an antiresonant behavior of cobalt-derived states at the $3p$-$3d$ excitation threshold. Information about the unoccupied density of states has been obtained by O K XAS. The structure of the Co L absorption edge is compared to semiempirical charge-transfer multiplet calculations. The experimental results are furthermore compared with band-structure calculations considering three different exchange potentials [generalized gradient approximation (GGA), using a nonlocal Hubbard U (GGA+U) and using a hybrid functional (Becke, three-parameter, Lee-Yang-Parr [B3LYP])]. For these different approaches total density of states and partial valence-band density of states have been investigated. The best qualitative agreement with experimental results has been obtained by using a GGA+U functional with U=2.9 eV.

DOI: 10.1103/PhysRevB.82.195431 PACS number(s): 68.47.Gh, 73.20.Hb, 79.60.Dp, 82.80.Pv

I. INTRODUCTION

$LiCoO_2$ and its alloys are still the most often used cathode materials in Li-ion batteries and its properties have been investigated by a wide variety of experimental techniques.[1–13] Due to its unique electrochemical and electronic properties the material has the character of a model system for fundamental investigations.

The high-temperature (HT) phase of $LiCoO_2$ crystallizes in a rhombohedral $R\bar{3}m(D_{3d}^5)$ structure.[14] The structure can be viewed as a cubic closed packed lattice of oxygen atoms with Co and Li alternately occupying the octahedral sites in the (111) planes. This ordering of the ions result in the so-called O3 layer structure with pure Li and Co layers separated by oxygen layers in an ABCABC stacking sequence displayed in Figure 1.

Due to its strong anisotropic crystal structure, the electronic structure of $LiCoO_2$ has some interesting properties: on one hand, localized Co $3d$ valence states are present, which give rise to strong electron correlation effects and hence complicated electron spectra. On the other hand, a sp-bandlike character of O $2p$ valence states can be observed. Moreover, a distinct covalent mixing of cobalt and oxygen states is present in the system,[15–17] resulting in charge-transfer processes in photoemission experiments.

Several studies on the electronic structure of $LiCoO_2$ have been published in the literature applying density functional theory (DFT) (Refs. 15 and 18–24) and cluster calculations[16,24,25] or electron spectroscopic techniques.[11,15,17,20,22–24,26–38] However, there are still aspects which need clarification, especially with respect to the relation between electrochemical behavior and the changes of the electronic structure during lithium extraction and insertion.[39]

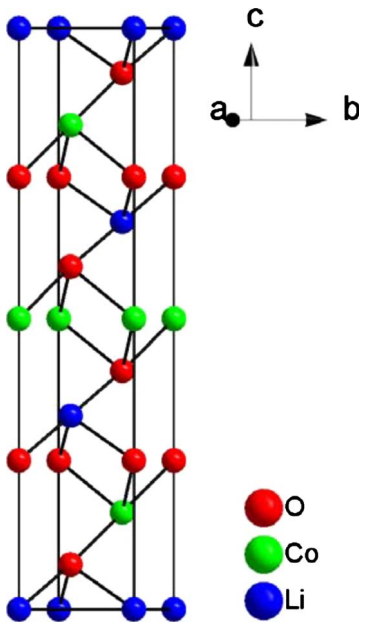

FIG. 1. (Color online) Illustration of the layered crystal structure of HT-$LiCoO_2$.

Contradictory descriptions about the electronic properties of $LiCoO_2$ can be found in the literature. The material has been classified as charge-transfer insulator,[17,24] insulator with negative charge-transfer energy,[26] Mott-type insulator,[21,40] or essentially a *p*-type semiconductor,[41,42] respectively.

An apparently complex defect chemistry of the material is reflected in discrepancies in the experimental band gap reported by several authors, which are also often used as basis for theoretical descriptions of the material. Ghosh *et al.*[43] estimated a band-gap value of 1.7 eV using optical spectroscopy for the HT phase of $LiCoO_2$. Kushida *et al.*[44] observed 2.1 eV for thin-film samples with ultraviolet-visible spectroscopy. A band gap of 2.5 eV has been found by Rosolen *et al.*[45] with photocurrent spectra. Van Elp *et al.*[24] determined a value of 2.7 eV experimentally by a combination of bremsstrahlung isochromat spectroscopy and x-ray photoemission spectroscopy (XPS) measurements.

A number of experimental studies focus on valence-band analysis by photoelectron spectroscopy (PES) (Refs. 10, 15, 17, 24, 26, and 30) and interpretation of conduction-band states using different electronic methods.[20,22,24,31,38,46,47] Usually, these studies are based on powder samples, which in some cases may lead to problems with the control of *extrinsic* and *intrinsic* impurity phases on their surfaces, in particular, for a valence-band analysis. Phases such as, e.g., carbon adsorbates and lithium compounds can be formed spontaneously on lithiated transition-metal oxides upon contact with air or during synthesis of the material. A detailed XPS/ultraviolet photoemission spectroscopy study on the formation of contamination phases on $LiCoO_2$ is reported elsewhere.[48]

From an experimental point of view, it is imperative for an interpretation of, e.g., valence-band structures to minimize unwanted, additional features in a spectrum. Hence, highly stoichiometric material and contamination free surfaces are demanded.

In order to meet these requirements the integrated ultrahigh vacuum (UHV) system for solid liquid interface analysis system (SoLiAS) at the synchrotron facility BESSY II in Berlin-Adlershof has been used, combining synchrotron x-ray photoemission spectroscopy (SXPS) analysis and *in situ* preparation by rf magnetron sputter deposition. This system enables a sample transfer between preparation and analysis without breaking UHV conditions.

There have been a number of studies published in the literature, which describe the preparation of $LiCoO_2$ as thin material for application in Li-ion batteries.[11,27,49–61] In particular, magnetron sputtering using a ceramic $LiCoO_2$ target has proven to be a successful method.[11,27,50–52,60,61]

Examples of a comparison between experimental XPS data and theoretical results can be found in the literature. Van Elp *et al.*[24] compared multiconfiguration model-Hamiltonian calculations for a CoO_6 cluster with experimental XPS data for $LiCoO_2$. In a study of Czyzyk *et al.*[15] the density of states (DOS) and partial density of states (PDOS) of $LiCoO_2$ have been calculated by a DFT band-structure calculation using a generalized gradient approximation (GGA) functional and compared with XP valence-band spectra taking into account experimental parameters and theoretical photoionization cross sections.[62] Kemp *et al.*[26] interpreted experimental results in terms of semiempirical band calculations and an impurity model.

In the present study the electronic structure of $LiCoO_2$ has been studied in detail by synchrotron-induced PES techniques. SXPS and resonant PES (ResPES) have been applied for an investigation of valence-band states. The near-edge structures of O *K* and Co *L* edges have been investigated by soft x-ray absorption spectroscopy (SXAS). The structure of the Co *L* edge has been compared to charge-transfer multiplet (CTM) calculations.

An experimental approach is presented, allowing the separation of oxygen- and cobalt-derived states based on synchrotron induced PES valence-band spectra. By applying ResPES, the partial density of states of the photoelectron final-state distribution can be obtained. The results of this approach are compared to theoretical predictions of the partial density of states in the valence-band region.

As it has been demonstrated for CoO,[63] calculated band widths and band gaps can depend significantly on the used exchange-correlation functional. Similar observations have been made for NiO, where the electronic properties depend strongly on the chosen functional and a good agreement with experimental data is found for the GGA+*U* functional.[64] The PDOS of $LiCoO_2$ has thus been calculated using three different functionals, namely, the GGA, GGA+*U* with different *U* parameters, and the hybrid functional B3LYP, a linear combination of a Hartree-Fock exchange potential, the Becke three parameters exchange potential, and the correlation potential of Lee, Yang, and Parr.[79]

II. EXPERIMENTAL

A. Film deposition and experimental equipment

The $LiCoO_2$ samples have been deposited by rf magnetron sputtering in a custom deposition chamber with a base pressure of 5×10^{-8} mbar.[11] The thin films were prepared from stoichiometric target material (99.9%, FHR Anlagenbau GmbH) on Ti-foil substrates (99.95%, Alfa Aesar) in an Ar/O_2 sputter gas mixture [Ar(5.0), O_2(4.8), Air Liquide]. During the deposition process the sample has been heated at 550 °C.

B. SXPS, SXAS and data normalization

The SXPS experiments have been carried out at a dipole beamline with the toroidal grating monochromator TGM7 at the synchrotron facility BESSY II, equipped with the integrated UHV system for SoLiAS combining different *in situ* preparation techniques with the surface-analysis system.[65] The spectrometer is equipped with the SPECS PHOIBOS 150 MCD-9 electron analyzer (base pressure 2×10^{-10} mbar). Photon energies in the range from $h\nu=25-120$ eV have been used with an overall energy resolution better than 100–300 meV. The binding energy scale for the spectra has been referenced to the Fermi level of a sputter cleaned Au reference sample. The use of low excitation energies results in strongly varying photoionization cross sections (Fig. 2) and surface sensitivity for valence-band studies.

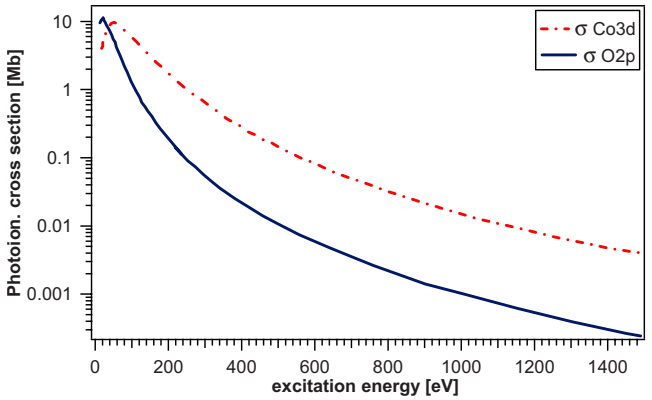

FIG. 2. (Color online) Photoionization cross sections reported by Yeh and Lindau (Ref. 62). Both orbitals have large contributions to the valence band of $LiCoO_2$.

For analysis of the resonant PES data, the intensities of the as measured valence-band spectra have been normalized to the incident x-ray flux on the refocusing mirror of the beamline as well as to the overall transmission function, which includes the sensitivity of the Phoibos electron analyzer (transmission function)[66] and the transmission of the optical elements of the beamline (monochromator, mirror transmission), and the energy-dependent inelastic mean free path λ of the electrons. A similar procedure has been applied for studies on the $Li_xV_2O_5$ system.[67] The spectral background due to inelastic electron scattering has been corrected by a Shirley-type background removal function.

For a comparison of the experimental data of the valence-band region with DFT calculations, the different photoionization cross sections of the Co 3*d*-, O 2*p*- (and Li 2*s*/2*p*-) derived states have been taken into account by normalizing the theoretical PDOS with values from Yeh and Lindau.[62] This procedure has already been demonstrated successfully by other authors.[15]

The SoLiAS system has also been used for XAS at the U49/II-PGM2 undulator beamline at BESSY II, analyzing the secondary electron yield as a function of the photon energy. The Co $L_{2,3}$ and O *K* edges have been probed to obtain information on unoccupied states. The accessible energy range at this beamline is $h\nu$=90–1900 eV with an overall energy resolution of better than 400 meV and about 150 meV below photon energies of 800 eV. Sputter cleaned Ag (E_F, 3*d*), and Au (4*f*) samples have been used for energy calibration. The experimental data has been compared to simulated x-ray absorption spectra. In case of Co $L_{2,3}$ absorption spectra CTM have been utilized.[68,69]

C. Computational details

For the calculation of the electronic structure of $LiCoO_2$ two different variants of DFT have been applied, namely, (a) the CRYSTAL06 program package[70] with linear combinations of atomic orbitals (LCAO) (Ref. 64 and 71) and (b) the Vienna *ab initio* simulation package (VASP) (Refs. 72–75) with projector augmented waves (PAW).[64,76] The electronic structure has been calculated using three different exchange-correlation functions, namely, the local GGA with the parameterization of Perdew *et al.*,[77] which is an appropriate method to describe the *sp* valence states, and a nonlocal screened Coulomb model *U* Hamiltonian, the GGA+*U* functional, based on Dudarev,[78] where the Co 3*d*-Co 3*d* interaction is described by the Hubbard *U* parameter. Furthermore, the widely used orbital dependent exchange potential B3LYP (Ref. 79) is applied as a mixture of DFT and Hartree-Fock exchange.

For the PAW calculations for Co the 4*s*, 3*p*, and 3*d* electrons, for O the 2*s* and 2*p* electrons and for Li the 1*s* and 2*s* electrons are treated as valence electrons. For the LCAO calculations the following basis sets were used: Li-6-111G*,[80] Co-86-411d41G,[81] and O-8-411G*.[82] Up to 216 *k* points in the Brillouin zone were utilized for integrations involving *k* space.

The calculations are based on the following structural parameters: a,b=2.82982(2); c=14.11900(44); and O_z =0.2562(6). These values are in good correspondence to the ones found in the literature[83,84] and have already been discussed in a previous study.[39] The negative deviation of the O_z parameter from 0.25 leads to a distortion of the octahedral oxygen surrounding of the cations. The LiO_6 octahedra are elongated with a Li-O bond length of 2.067 Å and two different O-O distances of 2.830 and 3.013 Å. The CoO_6 octahedra are compressed with a Co-O bond length of 1.963 Å and O-O distances of 2.830 and 2.791 Å. For the calculations the corresponding primitive cell with only one formula unit has been used. The structure optimization has been performed by the VASP program using the GGA functional as it is most efficient with respect to computing time.

III. RESULTS AND DISCUSSION

A. SXP valence band and constant initial state (CIS) spectra of thin film $LiCoO_2$

Valence-band spectra of *in situ* prepared $LiCoO_2$ thin films are shown in Fig. 3. The presence of the HT phase of $LiCoO_2$ has been confirmed for the thin films by XRD, Raman spectroscopy, and electrochemical measurements (not presented in this work). The films are highly crystalline and exhibit a strong (00*l*) preferential orientation when deposited on Ti foil. A detailed paper on the properties of sputter-deposited $LiCoO_2$ dependent on the preparation parameters is in preparation. In Fig. 4 a XP Al $K\alpha$ survey spectrum of a contamination free and stoichiometric $LiCoO_2$ thin film is shown. For reference Li 1*s*, O 1*s*, and Co $2p_{3/2}$ core-level spectra are also included in this figure. The valence-band structure of $LiCoO_2$ has been investigated experimentally by various authors.[10,15,24,29,30] In the upper valence-band region, around 1–3 eV in Fig. 3, a dominant Co 3*d* emission is observed, whereas the region between 3–10 eV is dominated by direct O 2*p* and O 2*p*/Co 3*d*-like contributions. Adjacent to this region at about 12 eV, a Co 3*d* final-state satellite is situated. It has been concluded that basically O 2*p* and Co 3*d* states contribute to the valence band DOS whereas Li 2*s*/2*p* contributions can be neglected in good approximation.

The SXP spectra have been measured at different excitation energies after UHV transfer from the preparation to the

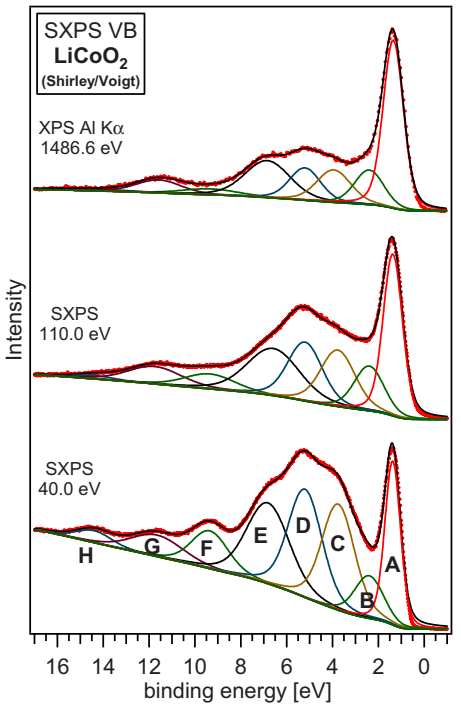

FIG. 3. (Color online) (s) XP valence-band spectra of clean rf-magnetron-deposited $LiCoO_2$ thin-film samples excitated at photon energies of 40 and 110 eV (SXPS), and 1486.6 eV (Al $K\alpha$), respectively.

analysis chamber. The use of different excitation energies allows a variation in the photoionization cross sections and the surface sensitivity. The valence-band emissions are approximated by a number of Gauss-Lorenz-shaped features (Voigt-type) named A-H, which allow reproducing the experimental spectrum for all excitation energies only by changing their relative intensities. Due to the different energy dependence of the excitation probability for oxygen, cobalt, and lithium orbitals in the valence-band-regime electron states with different atomic origin can be distinguished to a certain extent. Low excitation energies below 50 eV, for example, increase the sensitivity for oxygen-derived states, whereas Co states become dominant above 100 eV. The photoionization cross sections reported by Yeh and Lindau, although calculated for "free" atoms, will be used for this discussion.[62] In Fig. 2 the variation in cross sections versus excitation energy is shown for O $2p$ and Co $3d$ orbitals, which dominate the valence-band region (and conduction-band edge). By comparing XP spectra of $LiCoO_2$ taken at excitation energies of 40 eV and 1486.6 eV (Fig. 3), respectively, distinct variations in the relative intensities of the different emissions become apparent.

However, in addition to the differences in photoionization cross sections for O $2p$- and Co $3d$-derived valence-band states, the character of the latter can be investigated in more detail by CIS spectroscopy. The various resonant and nonresonant photoemission processes are discussed in detail in the Appendix. The excitation energy has been varied around the threshold energy for a Co $3p$-$3d$ excitation allowing autoionization processes (Fig. 5). The emissions A-G exhibit gradual changes in their resonant behavior (Fig. 6), which can be interpreted in terms of screening effects due to ligand-to-metal (L-M) charge transfer. Dependent on their resonant behavior, final states can be distinguished, which arise from an unscreened or weakly screened direct emission process or

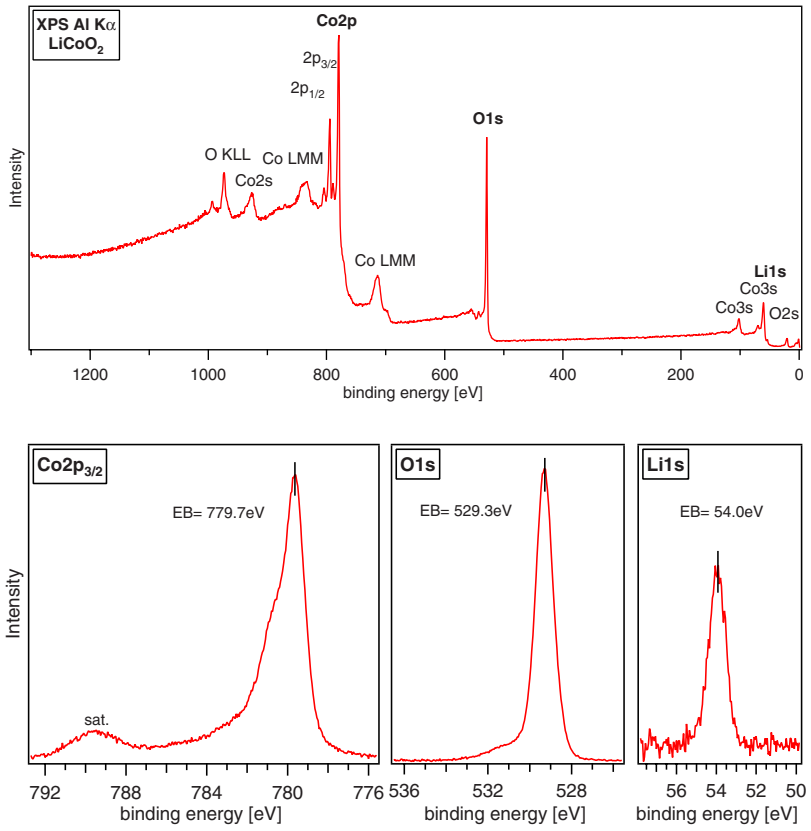

FIG. 4. (Color online) XPS Al $K\alpha$ survey spectrum of a $LiCoO_2$ thin film prepared by rf magnetron sputtering. The Co $2p_{3/2}$, O $1s$, and Li $1s$ spectra are given below.

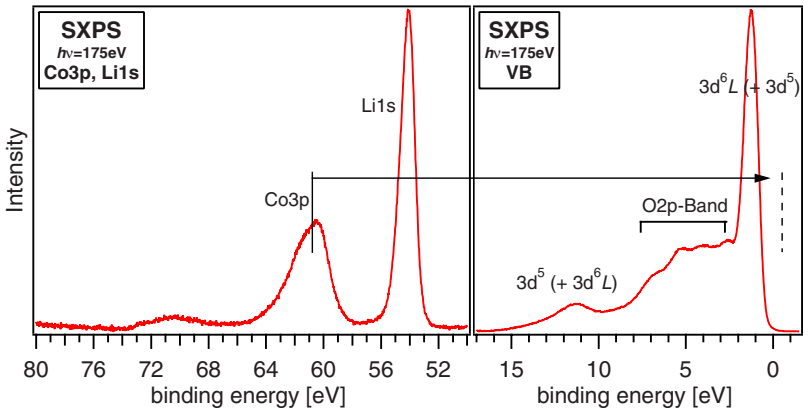

FIG. 5. (Color online) Illustration of the autoionization process for $LiCoO_2$ after exceeding the threshold energy for a Co $3p$-$3d$ excitation. The distance between the Co $3p_{3/2}$ (60.4 eV) level and the maximum of the Co $3d$ valence-band states (1.2 eV) is 59.2 eV. In Fig. 11 the corresponding resonant PES series of valence-band spectra is presented.

(partially) screened charge transfer transitions, respectively. For a screened charge-transfer final states an antiresonant behavior is expected, whereas an unscreened final state results in a resonance.[85]

For the measurements, shown in Fig. 6, a transition from a clear antiresonance in case of emission A to a moderate constructive resonance for emission G can be observed. The normalized data has been fitted with a Fano-type profile [Eq. (5)] including a linear correction (a^*E+b) to improve the fit quality by compensating slightly different slopes of the data before and after the resonance. The fit of the data yielded a resonance energy E_0 of 62 eV for emission A and slightly differing values of about 62.0 ± 0.5 eV for the other features (B–G), probably due to the Co $3p$ line width (Fig. 5). For the asymmetry parameter q values of 0.3 (A), 0.45 (B-E), 1.0 (F), and 1.25 (G) were found. For illustration Fano-type profiles are given in Fig. 7.

Taking into account the binding energy of the Co $3p_{3/2}$ core level of $E_B=60.4$ eV (Fig. 5), a p-d resonance energy of $E_R=62.0$ eV and a Fermi-level position of E_F-E_{VBM} $=0.7$eV a d-d band gap of about $E_g=E_R-E_B(\text{Co } 3p_{3/2})$ $+(E_F\text{-}E_{VBM}) \approx 2.3$ eV can be approximated, which is close to the value of 2.1 eV reported for thin films by Kushida *et al.*[44] This value, however, is not corrected for the full width half maximum (FWHM) of the peaks used for the estimation.

Based on the SXPS and CIS measurements the character of valence-band states can be discussed. The dominant emission at the valence-band edge at about $E_B(A)=1.2$ eV binding energy is mainly a screened Co $3d$-like emission (Co $3d^nL$). This feature does not correspond directly to t_{2g}-derived states ($^5D_{3d}$ symmetry) due to its charge-transfer character. However, since the photoinduced core hole is screened by the oxygen ligands, the binding energy of feature A is therefore close to the undisturbed t_{2g} states (and by this allows a comparison with DFT calculations of the ground state of the system). The small width of this feature of FWHM=0.7 eV at $h\nu=40$ eV is typical for low-spin Co^{3+} ions.[26] Emission B at $E_B(B)=2.4$ eV seems to be derived mainly from $3d$-like states as well. The broad band between $E_B(\text{C-E})=2.5-7.5$ eV binding energy, however, has a prevalent O $2p$-like character but still contains Co $3d$ admixtures to an appreciable extent. A poorly screened satellite is apparent at about $E_B(G)=12$ eV binding energy with a Co $3d^{n-1}$ character.[15] However, contributions of a $d^{n+1}L^2$ configuration might be present as well in the satellite feature, which are also higher in energy due to extra repulsion between the additional holes.[26]

Emissions due to traces of Li_2O_2 at the sample surface are visible at low excitation energies at $E_B(F)=9.5$ eV and $E_B(H)=14.5$ eV, respectively. A paper investigating spectral

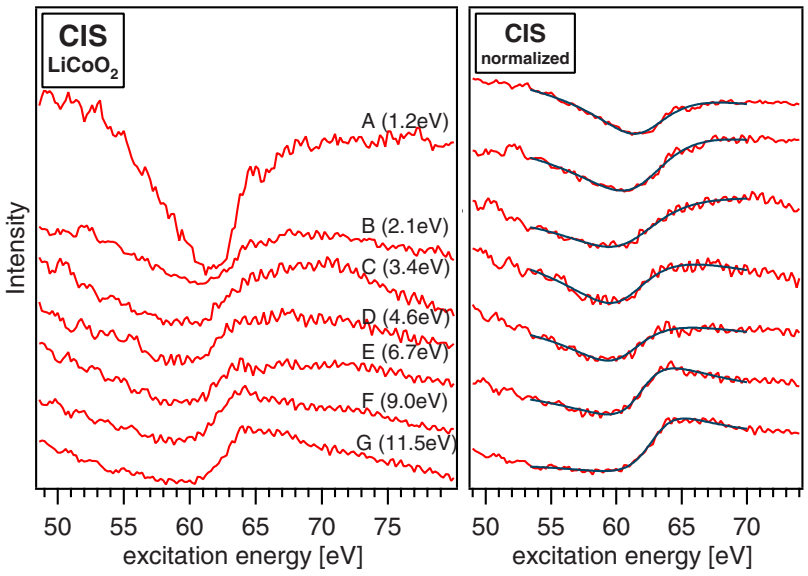

FIG. 6. (Color online) CIS measurements at different positions in the valence band of $LiCoO_2$. The binding energies of features A–G are indicated (see also). The right plot shows the same data normalized to unity and fitted with a Fano-type profile.

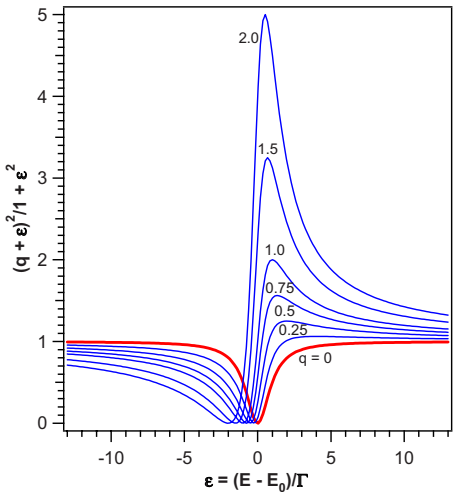

FIG. 7. (Color online) Fano profiles plotted for different values of the asymmetry parameter q with $\Gamma = 1$ eV.

features of surface contamination phases in the valence band region is published elsewhere.[48]

It should be noted that satellite feature (G) cannot be described within the single-particle treatment of the DFT calculations as excitation processes within the valence-band states are involved leading to different final-state occupation of valence-band states. Obviously, the same applies for emissions F and H.

B. Electronic-structure calculations of $LiCoO_2$

The electronic structure of $LiCoO_2$ has been calculated both in a spin restricted and spin unrestricted way, which lead to the same nonmagnetic ground state. In Fig. 8 a comparison of the band structure of $LiCoO_2$ is given, obtained from the three different potentials, GGA, GGA+U, and B3LYP, mentioned above. In order to allow a direct comparison with the experimental data, the energy scale is referenced to the Fermi energy E_F, which was arbitrarily set in the middle of the band gap. The ordering of the states is most clearly seen for the GGA potentials in Fig. 8(a). These results are similar to the work of Czyzyk *et al.*[16] The six bands between −8 and −3 eV are 2p-like bands of oxygen. These bands are separated by a small energy gap from the three occupied 3d-like states of cobalt located between −2 and −1 eV. This small energy gap disappears when using the other functionals. For the GGA+U the overlap of O 2p- and the Co 3d-derived bands correlates directly with the chosen U parameter: A higher value of U results in a stronger overlap [Figs. 8(b) and 8(c)].

The size of the optical band gap between the occupied and unoccupied 3d-like states of cobalt depends of course significantly on the chosen functional. The predicted band gap of 1.2 eV for the GGA functional is much smaller than the experimental value of 2.1 eV for thin films.[44] This underestimation of the band gap is usually found from a DFT approach.[87]

For GGA+U the size of the optical band gap depends sensitively on the chosen U parameter. The proposed U parameter of U=4.91 eV for Co 3d orbitals of Marinetti *et al.*[19] yields a larger band gap of 2.7, which matches the experimental value reported by van Elp *et al.*[24]

In the present study a U parameter of 2.9 eV has been chosen for the GGA+U calculation. This value reproduces the experimental value of 2.1 eV (Ref. 44) for the optical band gap and is in accordance with our estimate in the previous section. As it will be shown below, the choice of 2.9 eV for the U parameter not only reproduces the optical band gap quite well but also gives the best qualitative agreement between the experimentally and theoretically derived valence band density of states of $LiCoO_2$, shown in Fig. 19 in Sec. V.

For the hybrid potential B3LYP, however, the predicted optical band gap of 4.2 eV is significantly larger than the experimental value. In Fig. 9 the partial DOS (PDOS) $n_\nu(E)$ associated to the atoms ν and $n_{\nu,l}(E)$ additionally associated to the angular momentum l is displayed for Co s-, p-, and d-like states and O s, p-like states is displayed (note the different scaling for the various columns in the PDOS). From the n_ν(E) plots the character of the chemical bonds can be deduced: first, there is almost no contribution of Li supporting an almost pure ionic character of Li in this compound. Second, in the energy range of the 2p-like states of oxygen (GGA: from −8 to −2.6 eV, and GGA+U (U=2.9 eV): from −7.5 to −2.3 eV, and GGA+U (U=4.91 eV): from −7.5 to −2.9 eV, and B3LYP: from −9 to −3.5 eV) also distinct amplitudes in the partial DOS of Co can be found and vice versa. Thus, noticeable covalent contributions to the Co-O bonds are indicated. However, only small oxygen contributions are observed in the energy range of the 3d-like cobalt states close to the valence-band maximum (GGA:

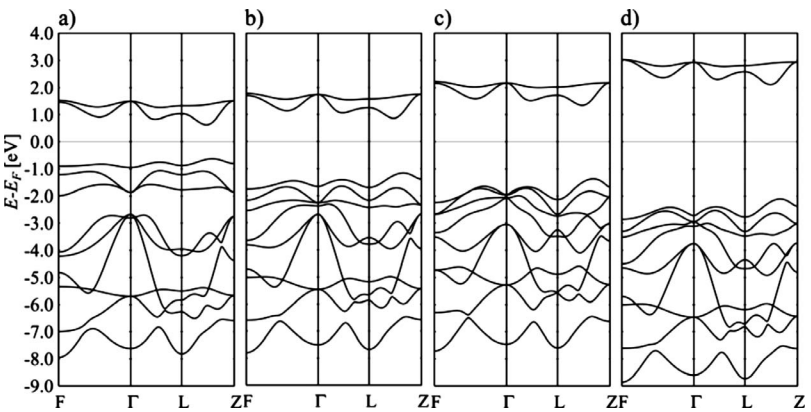

FIG. 8. Electronic band structure of $LiCoO_2$ along selected symmetry lines, see Bradley and Cracknell (Ref. 86), for the trigonal lattice. The energy scale is referenced to the Fermi Energy. (a) GGA, (b) GGA+U (U=2.9 eV), (c) GGA +U (U=4.91 eV), and (d) B3LYP.

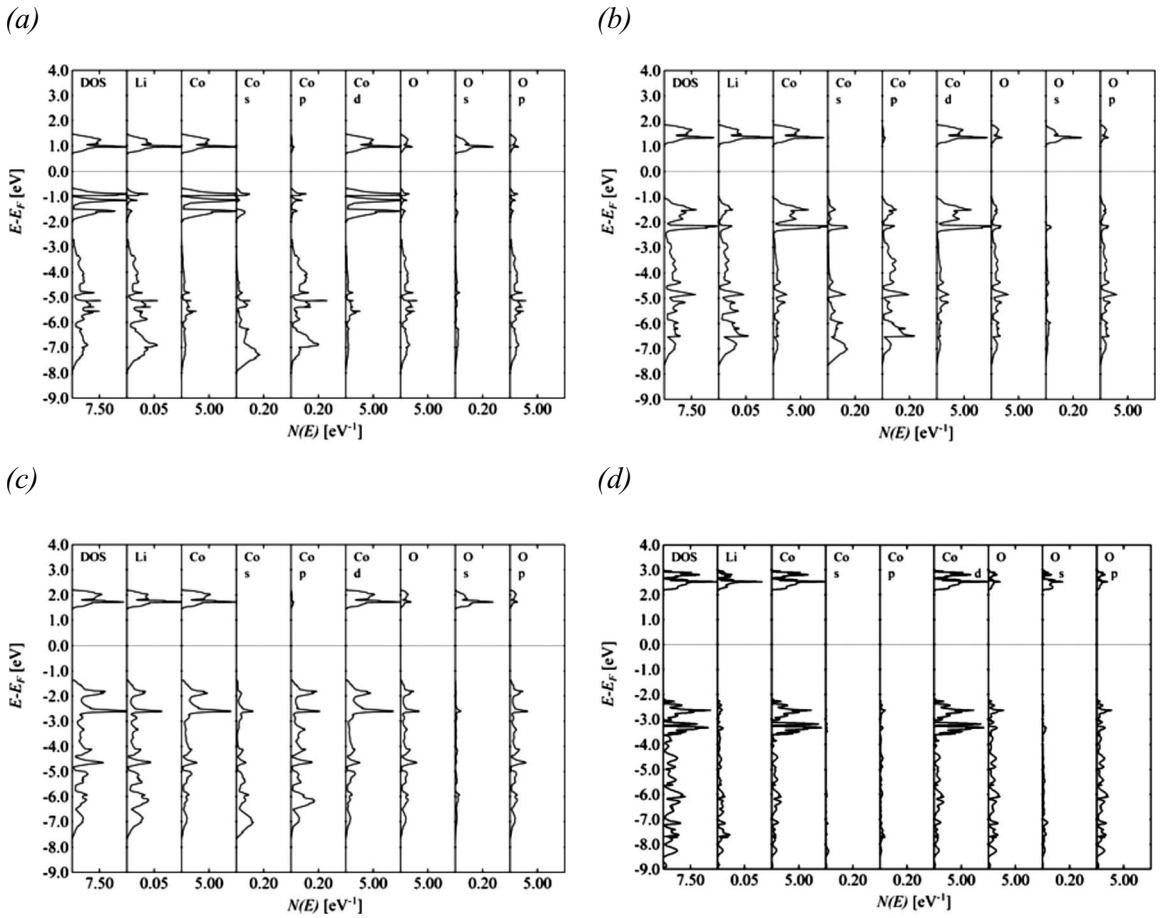

FIG. 9. Total DOS $n(E)$ and partial DOS $n_{\nu,\mathrm{l}}(E)$ of $LiCoO_2$, with ν=Li, Co, O, and l=s,p,d. The data is obtained from (a) GGA, (b) GGA+U (U=2.9 eV), (c) GGA+U (U=4.91 eV), and (d) B3LYP calculations.

−0.6 to −2 eV, GGA+U (U=2.9 eV): −1 to 2.3 eV, GGA +U (U=4.91 eV): −1.3 to 2.9 eV, and B3LYP: −2.1 to 3.5 eV). In this narrow energy range of the upper valence band the Co 3d character is dominating, resulting in a more localized nature of these cobaltlike states compared to the much broader, bandlike O 2p/Co 3d states forming the lower valence band. Third, since the $n_{\nu,\mathrm{l}}$(E) contributions of Co s-, p-, and O s-like states are very small for the shown energy range, an almost pure d-like and p-like characters can be assumed for cobalt and oxygen states, respectively.

For the GGA and GGA+U calculation [Figs. 9(a)–9(c)], small amplitudes of Co s- and p-like states are visible in the DOS, which are negligible for the B3LYP calculation [Fig. 9(d)]. There is no amplitude of O s-like states for the occupied states in this energy region; however, a small contribution of O s-like states can be seen for the unoccupied states.

The partly covalent character of the bonds between oxygen and cobalt is also reflected in the charge-density distribution $\rho(r)$ in Fig. 10, displayed for the GGA+U (U =2.9 eV) calculation [Fig. 9(b)]. For illustrative reasons, the $2\times2\times1$ supercell of Fig. 1 has been used and an identical color scale has been chosen for the three different energy ranges.

In Fig. 10(a), $\rho(r)$ is shown for the energy range between −8 and −2.5 eV. The covalent Co-O bond contributions are indicated by charge bridges between cobalt and oxygen atoms. Between −2.5 and −1 eV the 3d-like character of the cobalt orbital forming the upper valence band is clearly evident with only a very weak bond to the oxygen [Fig. 10(b)]. The unoccupied states for the energy range between 1 and 2 eV are shown in Fig. 10(c). Again, the charge density around cobalt is shaped like a 3d orbital, namely, t_{2g}-like occupied

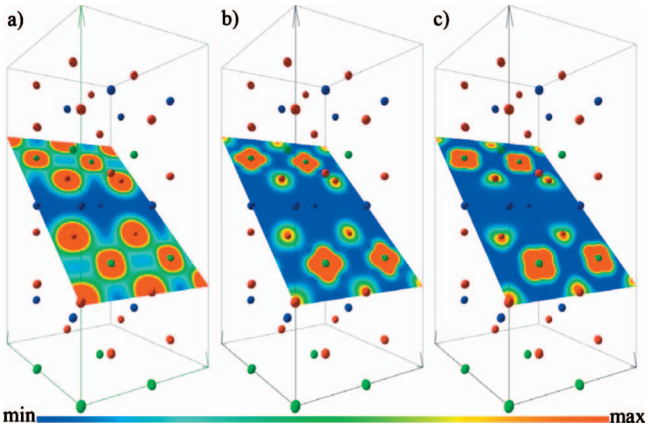

FIG. 10. (Color) Charge density ρ(r) of $LiCoO_2$ obtained from a GGA+U calculation with U=2.9 eV for different energy ranges: (a) −8 to −2.5 eV (covalent bonds), (b) −2.5 to −1 eV (t_{2g}), and (c) 1–2 eV (e_g). Li atoms are colored blue, Co atoms green, and O atoms red.

states [Fig. 10(b)] and e_g-like unoccupied states [Fig. 10(c)]. In all three figures, a–c, no charge density around the blue-colored Li atoms can be observed indicating Li^+ ions.

C. Resonant photoelectron spectroscopy: Experimental derivation of partial valence-band density of states (PVBDOS)

ResPES has been applied in order to investigate the electronic structure of $LiCoO_2$ thin films experimentally in more detail. The technique delivers unique insights in the electronic structure of the valence band of a material since the occupied partial density of states can be studied.[88,89] As already shown for the CIS technique, information about bonding character, hybridization and photoelectron final states can be obtained. ResPES was first applied by van Elp *et al.*[24] to study electronic properties of $LiCoO_2$. The authors also observed an antiresonance of the Co 3*d* states (feature A in Fig. 3). For the satellite feature at about 12 eV (G), in contrast to our results (see Sec. IV A), again an anti resonant behavior has been reported. In this study resonances of cobalt states are further utilized in a new approach for an experimental separation of oxygen- and cobalt-derived valence-band states of $LiCoO_2$. An advantage of this procedure over x-ray emission studies is the better spectral resolution in photoemission experiments.

A series of $LiCoO_2$ valence-band spectra has been recorded by varying excitation energies between 25 and 120 eV (Fig. 11). For analysis of the data a similar treatment as reported earlier for Na/V_2O_5 has been applied.[67] The data have been normalized with respect to experimental conditions and the general dependence of the photoionization cross sections.

As for the case of V_2O_5 the normalization is based on the following approximate relation for the intensity (density of states approximation):

$$I(h\nu,E_B) \propto n_{ph}(h\nu)\cdot\lambda[E_{kin}(h\nu)]\cdot T[E_{kin}(h\nu)]\cdots \times\left[\frac{\sigma_{O\,2p}(h\nu)}{\bar{\sigma}(h\nu)}n_{O\,2p}(E_B)+\frac{\sigma_{Co\,3d}(h\nu)}{\bar{\sigma}(h\nu)}n_{Co\,3d}(E_B)\right]. \quad (1)$$

In this equation is n_{ph} the photon flux of the monochromator, measured as photocurrent at the refocusing mirror of the monochromator, λ the inelastic mean free path of the electrons, T the transmission function of the PHOIBOS electron analyzer, and $\bar{\sigma}$ the mean value of the photoionization cross section of the valence-band approximated from the cross sections $\sigma_{O\,2p}$ (66.6%) for O 2*p* and $\sigma_{Co\,3d}$ (33.3%) for Co 3*d* contributions. These influences on the spectral intensity are illustrated in [Figs. 12(a)–12(d)]. The terms $n_{Co\,3d}(E_B)$ and $n_{O\,2p}(E_B)$ represent the partial density of cobalt and oxygen states in the valence band (PVBDOS), see Fig. 9.

In the case of V_2O_5 a separation of V 3*d* and O 2*p* states has been achieved by subtracting an off-resonance spectrum ($h\nu$=43 eV) before the resonance and a spectrum in resonance ($h\nu$=54 eV). By this procedure, the O 2*p* contribution has been eliminated and thus the V 3*d* contribution is separated. Details are reported elsewhere.[67]

In contrast to V_2O_5, however, $LiCoO_2$ reveals an antiresonant behavior, which apparently cannot be used for an elimination of contributions of oxygen states in a similar way. Therefore, in the special case of an antiresonance of cobalt-derived states in $LiCoO_2$ a new procedure has been applied. The intensity devolution as function of excitation energy is plotted for the Co 3*d* main emission at 1.2 eV and a predominant oxygenlike emission at 5.0 eV in Fig. 13(a). For demonstrative reasons the data are shown prior to the data normalization described before. Thus, the gradual change in the intensity is governed by the energy dependence of photoionization cross sections and experimental factors (Fig. 12), which are indicated by an empirical function. At around 62 eV a modulation in the intensity is observed due to a Co 2*p*-3*d* resonance effect (see also CIS data, Fig. 6).

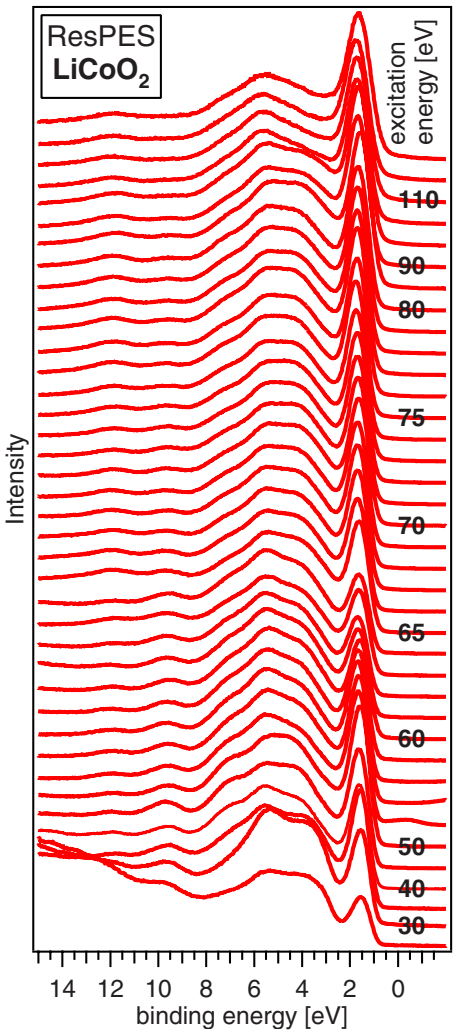

FIG. 11. (Color online) Normalized data of a resonant PES series of the $LiCoO_2$ valence band for excitation energies varied between 25 and 120 eV.

For a separation of states with predominant Co 3*d* origin, which are resonating, a spectrum $\bar{S}_{oR}(a,b)$ has been generated at the 2*p*-3*d* resonance threshold *without* a resonant modulation (*off-resonance*, oR) by taking an average of spectra before $S(a)$ and after $S(b)$ the resonance. For statistical reasons a number of symmetric $S(a)$, $S(b)$ pairs have been chosen around the excitation energy, at which the resonance occurs, as indicated in Fig. 13(a). It has been assumed that

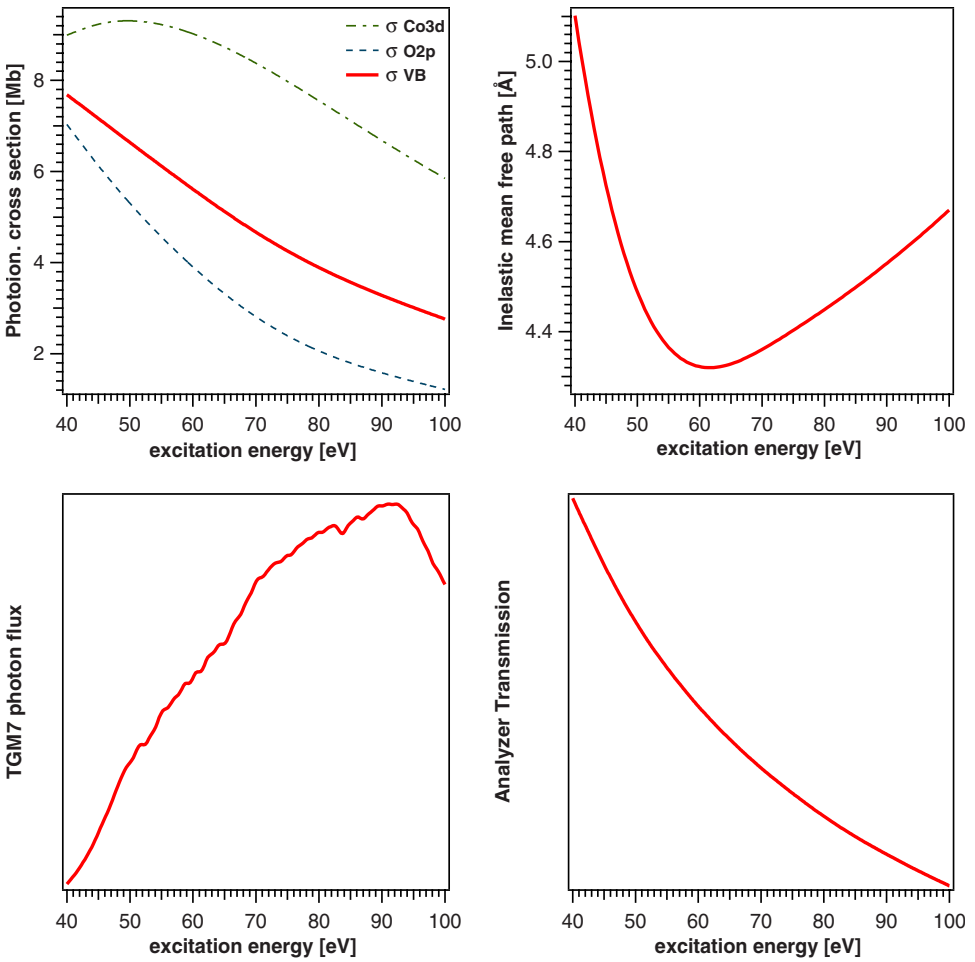

FIG. 12. (Color online) Contributions to the photoelectron intensity of valence-band spectra: (a) photoionization cross sections (Ref. 62), (b) inelastic mean-free path (Ref. 90), (c) TGM7 photon flux, and (d) transmission function of the electron analyzer (Ref. 66).

the spectra with a distance of more than 7 eV from the resonance are not affected by it. The procedure is expressed in the following equation:

$$\bar{S}_{\mathrm{oR}}(a,b) = \sum_i \frac{S_{\mathrm{oR},i}(a,b)}{i}. \tag{2}$$

By subtracting the experimental spectrum S_R at the resonance ($h\nu$=62 eV) from the calculated spectrum without (anti-) resonant contributions $\bar{S}_{\mathrm{oR}}(a,b)$, see Figure 13(b), it is possible to separate the resonant contribution, i.e., Co 3d-derived states ($S_{\mathrm{Co}\ 3d}=\bar{S}_{\mathrm{oR}}(a,b)-S_R$). The O 2$p$-like states are then generated by simply subtracting the cobalt contribution $S_{\mathrm{Co}\ 3d}$ from the actual spectrum S_R at the 2p-3d threshold ($S_{\mathrm{O}\ 2p}=S_R-S_{\mathrm{Co}\ 3d}$).

The final result, the partial state contributions of Co 3d- and O 2p-derived states in the valence-band region of $LiCoO_2$, is presented in Fig. 14. In order to prove the validity of this procedure, a $LiCoO_2$ valence-band spectrum measured with Al $K\alpha$ radiation (1486.6 eV) is included in this plot. At this photon energy the Co 3d photoionization cross section is about 20 times larger than for O 2p states.[62] Thus,

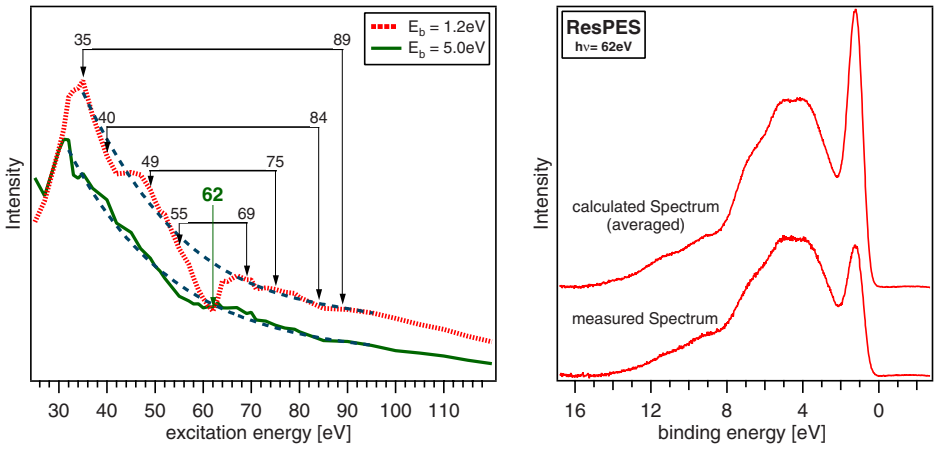

FIG. 13. (Color online) (a) Illustration of the procedure to generate an off-resonance spectrum (S_{oR}) at the resonance energy. The intensity devolution of the Co 3d-like main valence-band emission at E_B=1.2 eV shown as well as an emission at E_B=5.0 eV with a predominant O 2p-like origin. See text for details. (b) Comparison of the generated off-resonance spectrum and the actual spectrum both measured at $h\nu$=62 eV.

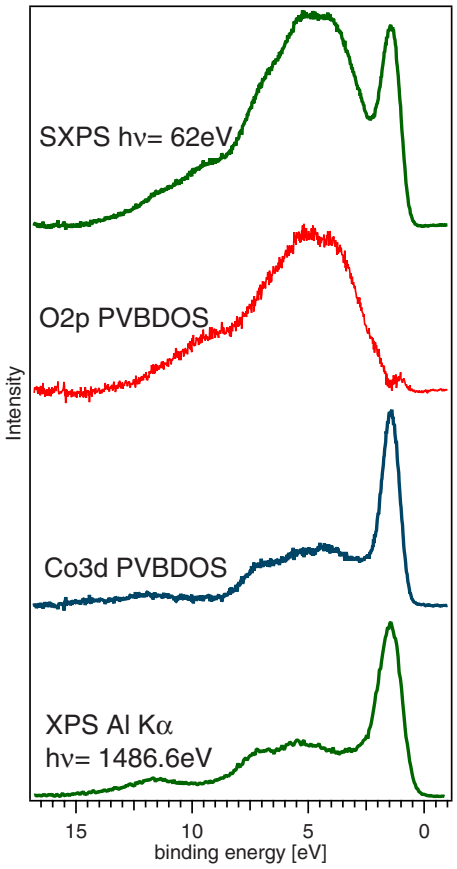

FIG. 14. (Color online) Experimentally derived PVBDOS of $LiCoO_2$. Oxygen- and cobalt-derived contributions have been separated based on resonant PES measurements. For comparison, a valence-band spectrum measured with Al $K\alpha$ radiation is included. A very good resemblance between separated Co 3*d* states measured at 62 eV and the XPS valence band of $LiCoO_2$ measured at 1486.6 eV is apparent. At this energy the photoionization cross section of Co 3*d* states is about 20 times higher than for O 2*p*-like states.

virtually only cobalt states are visible in the valence-band spectrum. A good agreement between the separated Co 3*d*-like states measured at 62eV ($S_{\mathrm{Co}\,3d}$) and the Al $K\alpha$ spectrum is clearly evident.

D. X-ray absorption spectroscopy: Experimental investigation of conduction-band states

XAS has been applied in order to obtain information about unoccupied states of $LiCoO_2$ thin films. The Co $L_{2,3}$ and O *K* edge have been measured in partial electron yield (PEY) detecting electrons with a kinetic energy of 200 eV.

Near-edge structures (XANES) of *K* edges are usually considered to be closely related to the empty density of states of the material. In case of O *K* edge the O 2*p*-projected density of states can be investigated since the spectra basically reflect transitions from the O 1*s* core level to unoccupied O 2*p*-derived states. According to de Groot *et al.*[91] the O *K* XANES region of 3*d*-metal oxides can be separated in two regions. The sharp features at the leading edge result from oxygen 2*p* orbitals hybridized into metal 3*d* states. About

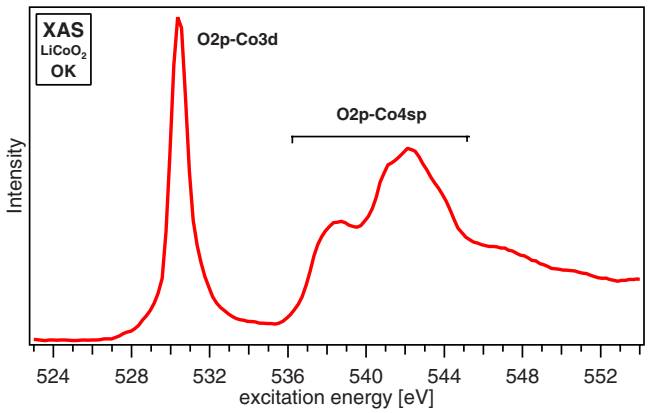

FIG. 15. (Color online) X-ray absorption spectrum of the O *K* edge of $LiCoO_2$.

5–10 eV above the edge broad structures can be observed due to transitions in oxygen-derived states hybridized with metal 4*s*- and 4*p*-like character.[24,91]

In dipole approximation ($\Delta l = \pm 1$), the shape of the absorption spectrum should represent the partial density of empty states projected on the absorbing atom (convoluted with Lorenzian spectral broadening due to limited lifetime of the core hole). However, also contributions from quadrupole transitions can be observed as pre-edge features.

The O *K* edge of HT-$LiCoO_2$ is shown in Figure 15. For stoichiometric material a low spin configuration of Co^{3+} ions is present in this modification (t_{2g}^6, $^1A_{1g}$). The sharp main line A at 530.6 eV corresponds to transitions of an O 1*s* electron in unoccupied states with a mixed Co 3*d*(e_g)-O 2*p* character and can be described as a O $1s^1c$+Co $3d^7(t_{2g}^6e_g^1)$ final states (where *c* denotes an O 1*s* core hole). The structures above 535 eV have been attributed to transitions in Co 4*s* and 4*p*-derived states with O 2*p* admixtures.[20,91] The large extension of O 2*p* states up to 15 eV above E_F,[15] indicates a strong covalency of the Co-O bond. The maxima of the 4*sp*-O 2*p* hybrid band are observed at 538.7 eV (B) and 542.4 eV (C). According to de Groot *et al.*[91] these structures result from the O_h-like symmetry of the oxygen neighbors coordinating the transition-metal ions.

The hybridization of cobalt and oxygen states leads to an admixture of O 2*p* states to the unoccupied conduction-band states with predominantly Co 3*d* characters. In a purely ionic model the electron configuration of oxygen would be O $1s^22s^22p^6$, hence no dipole transition O $1s \rightarrow$ O 2*p* would be possible. Only due to the covalent bonding a ligand-to-metal charge transfer can occur, allowing 1*s*-2*p* transitions. The intensity of the O *K* absorption edge is dependent on the amount of "*d*-hole states" in the 3*d*-2*p* hybrid orbitals and thus proportional to the O 2*p* character in the conduction band. Therefore, it can be seen as indicator for the degree of covalency in the CoO_6 octahedron.

The Li *K* absorption edge of $LiCoO_2$ is presented in Fig. 16 along with the Li 1*s* core level and the Co $M_{2,3}$ edges. The binding energy of the Li 1*s* peak is E_B(Li 1*s*) =54.0 eV, the maximum of the Li *K* has been observed at 55.4 eV and for the Co $M_{2,3}$ edges at around 58.1 eV and 59.2 eV, respectively.

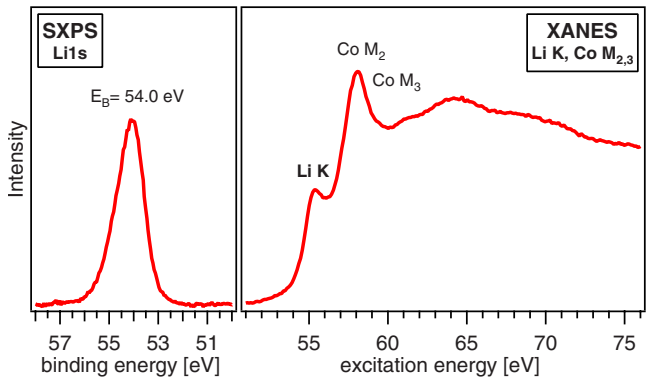

FIG. 16. (Color online) Li1s SXP and SXA spectra of $LiCoO_2$ thin films. The SXAS data also contains the Co $M_{2,3}$ edges.

A comparative illustration of the O K and Co L_3 edges of $LiCoO_2$ is given in Fig. 17. The common energy scale of the XAS data has been obtained by referencing the excitation energy to the respective O 1s and Co $2p_{3/2}$ core-level emissions. In contrast to the K edges, the $L_{2,3}$ edges of transition-metal oxides are largely influenced by crystal field multiplet effects and hence do not represent the density of states directly.[69]

The absorption spectrum of the Co $L_{2,3}$ edges of $LiCoO_2$ is shown in Figure 18(a) and has been compared CTM, Figures 18(b) and 18(c). For the calculations the D_{3d}^5 symmetry of $LiCoO_2$ (Ref. 14) has been simplified and a O_h symmetry assumed for the crystal field of Co^{3+} ions in the CoO_6 octahedra, neglecting the slight distortion of the lattice.

The CTM code, developed by Stavitski and de Groot,[68,69] includes charge-transfer multiplet theory (which allows more than one configuration) and ligand field multiplet theory (which includes the symmetry information). The main empirical parameters for the simulation of x-ray absorption spectra are the crystal field splitting 10Dq, the charge-transfer gap Δ, which gives the energy difference between the $3d^n$ and $3d^{n+1}L$ configurations, the difference between Hubbard U and the core-hole potential U_{3d3d}-U_{2p3d} and the

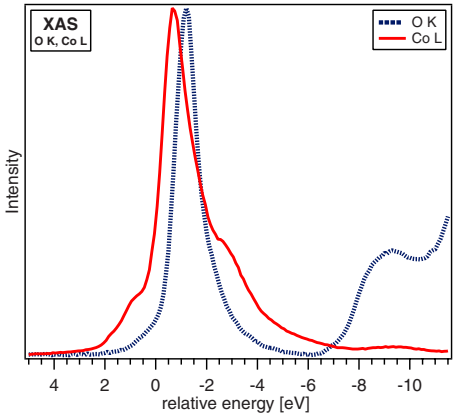

FIG. 17. (Color online) X-ray absorption near-edge structures of $LiCoO_2$ thin films for (a) O K, dotted and (b) Co L_3 edges, solid. The excitation energy has been referenced to the Fermi energy in a common energy scale based on the position of the respective O 1s and Co $2p_{3/2}$ core-level emissions.

hopping parameters T, describing the mixing between e_g and t_{2g} orbitals. In case of O_h symmetry $T(e_g)=2T(t_{2g})$ can be assumed. The slater integrals have been reduced to 80% of the Hartree-Fock value. A comprehensive overview of the parameters and the underlying model is given by Bocquet *et al.*[92]

A ligand field calculation (LF) without charge transfer effects is shown in Figure 18(b). In this case a crystal field splitting of $10Dq=2.2$ eV has been used. The LF calculation allows to reproduce the basic features of the experimental data and is in good agreement with simulated spectra published by Montoro *et al.*[22] using a similar approach.

However, a better qualitative agreement between experiment and theory has been achieved by taking charge-transfer processes into account. The empirical parameters for the charge-transfer multiplet approach (LF+CT), shown in Fig. 18(c), are $10Dq=1.5$ eV, $\Delta=1.5$ eV, U_{3d3d}-$U_{2p3d}=-1.5$ eV, and $T(e_g)=2.35$ eV. Here, the fine-structure and shape of the L_3 and L_2 main lines is approached more closely. In particular, the weak satellite feature at about $\Delta E=+8.8$ eV relative to the main lines can only be described by the LF+CT calculation.

A good agreement between theory and experiment suggests that there is a considerable covalent mixing of O 2p and Co 3d states above and below E_F and is in accordance with the band structure results presented in Sec. IV B. Considering the theoretically derived values for Δ ($\Delta^{CTM}=1.5$ eV) and U ($U^{GGA+U}=2.9$ eV) $LiCoO_2$ can be classified as a charge-transfer compound in the Zaanen-Sawatzky-Allen (ZSA) diagram.[93]

IV. COMPARISON OF EXPERIMENTAL AND THEORETICAL RESULTS

A. Partial density of valence-band states derived by GGA+U and ResPES

A comparison between the experimental partial density of valence-band states derived by ResPES ($h\nu=62$ eV) and the theoretical results based on GGA+U with $U=2.9$ eV is presented in Fig. 19. The theoretical data has been normalized with theoretical cross sections[62] and convoluted with a Gaussian line shape of half width 0.4 eV. The theory reproduces basic features of the experimental spectrum to a reasonable extent. The structure found theoretically for the Co 3d main emission disappears because of the Gauss smearing. Differences between experimental and theoretical curves are the missing satellites in the calculated DOS, which are discussed above, and variations in the relative contributions of oxygen and cobalt derived states which can be observed for the upper and lower valence-band region. In the calculation the small but noticeable admixture (hybridization) of Co 3d and O 2p states in the upper valence band (0–2 eV) leads to a partial density of Co states of about 85% and about 15% O 2p states. In the experimental data the O 2p fraction for this peak is notably smaller, about less than 5%.

This discrepancy might be originated in the DFT calculation by the use of the functional, the arbitrariness in the chosen atomic radii, the contribution of final state effects as

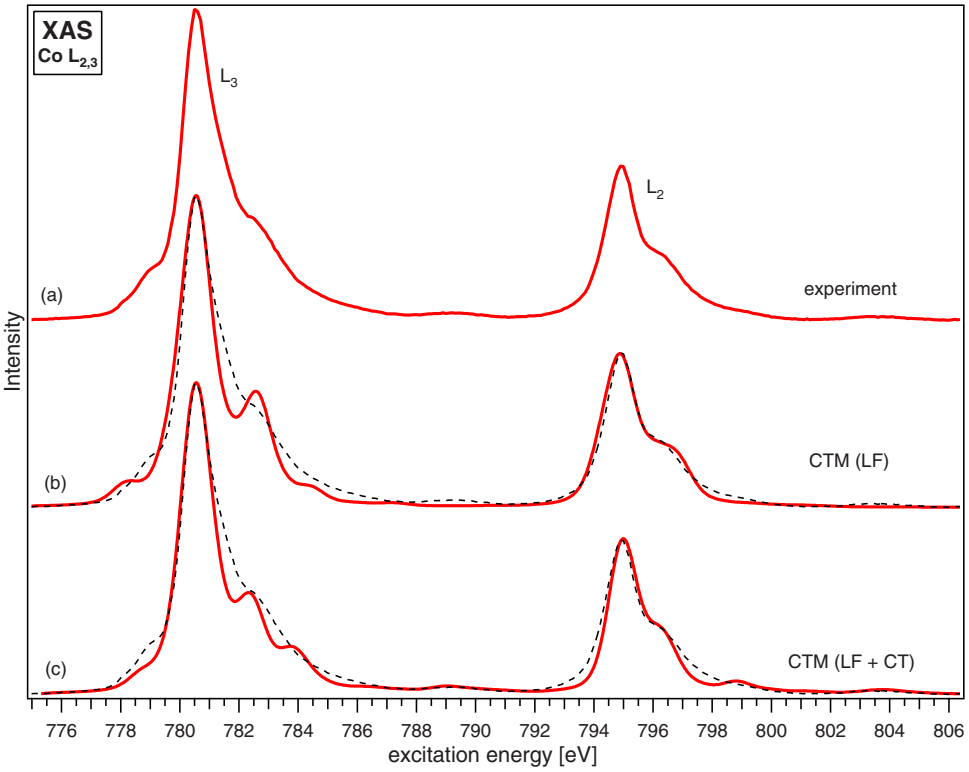

FIG. 18. (Color online) Experimental spectrum of (a) Co $L_{2,3}$ XANES compared to (b) ligand field multiplet calculations by the CTM method (LF) and (c) charge-transfer multiplet calculations by the CTM method (LF+CT). The best qualitative agreement with the experimental spectrum (dashed curves) has been achieved including charge-transfer effects. The parameters used for the simulated spectra are discussed in the text.

discussed above and furthermore the use of theoretical cross sections for the normalization, which can only represent an approximation. The gradual changes in the screening behavior observed in the CIS measurements (Sec. IV A) results in a "smearing-out" effect of the 3*d* states: partially screened or unscreened of the 3*d* states are shifted to higher binding energies compared to the undisturbed ground state (final-state effect).

B. Comparison of theoretical and experimentally derived valence- and conduction-band states of $LiCoO_2$

Finally, the experimentally derived electronic structure is compared to the DFT calculations (GGA+U, U=2.9 eV) in Fig. 20. For this illustration SXP valence-band ($h\nu$ =175 eV) and SXAS conduction-band spectra (O K edge) have been aligned on a common energy scale. The intensity of the SXAS and SXPS data is normalized with respect to the main peaks in the spectra. In this case no further cross-section correction has been applied to the DFT data.

A reasonable agreement in the alignment of O 2*p*- and Co 3*d*-derived states is achieved in the valence-band and the lower conduction-band states. However, the calculation differs notably in the energetic position of the O 2*s* core level and the Co 4*sp*/O 2*p* conduction-band states. In this case a dynamic many-body interaction theory is required for a more appropriate description as Czyzyk *et al.* already pointed out.[15]

V. CONCLUSION

In this work detailed information about the bonding character, hybridization and the position of photoelectron final states has been obtained for $LiCoO_2$ by applying different photoelectron spectroscopy techniques. The analysis of

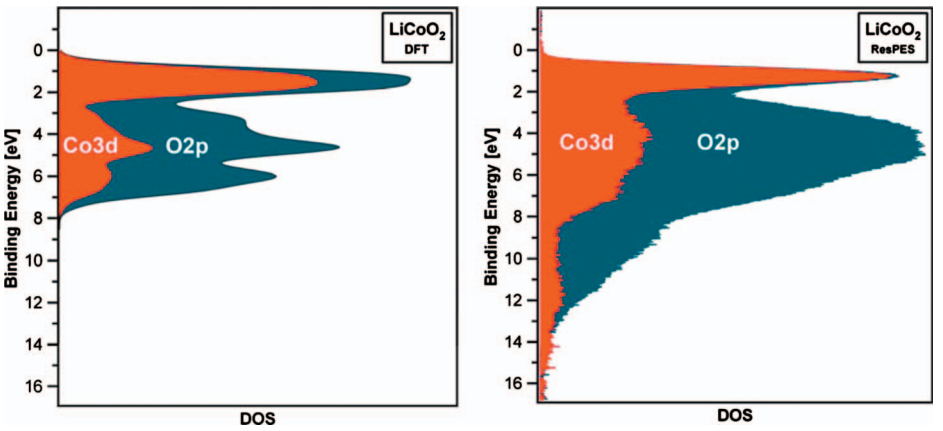

FIG. 19. (Color) Comparison of PVBDOS derived experimentally by resonant photoelectron spectroscopy and DFT calculations (GGA+U, U=2.9 eV).

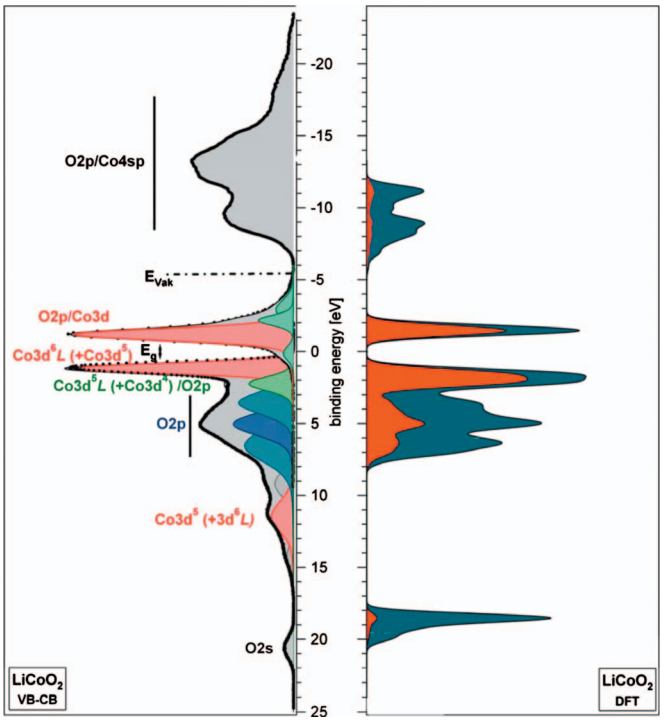

FIG. 20. (Color) Comparison of the experimentally deduced electronic structure of $LiCoO_2$ and the theoretical DOS (density of states) based on DFT calculations (GCA+U, U=2.9 eV). For this illustration SXP valence band ($h\nu$=175 eV) and SXAS conduction band spectra (O K edge) have been aligned on a common energy scale.

valence-band states by SXPS, CIS facilitated an identification of different final-state contributions. Furthermore, resonant and nonresonant contributions have been separated by ResPES and the partial density of O $2p$ and Co $3d$ states deduced. By XAS information about unoccupied states has been derived. The results have been compared to DFT-based calculations.

An accurate description of photoelectron spectroscopy data of correlated systems with theoretical techniques remains a challenging task. The band gap of $LiCoO_2$ as well as the alignment of valence and conduction bands can be "fitted" by introducing electron correlation effects with the Hubbard U parameter. However, beyond this approximation a dynamic many-body response theory would be required to describe photoionization processes accurately.

Nevertheless, a comparison between experimental results and calculations gives a reasonable agreement for the system $LiCoO_2$. Due to the charge-transfer processes and screening effects the observed valence-band structure are close to the ground state of the system. From a spectroscopic point of view the character of valence electrons lies in between transient and itinerant electrons for this system.

ACKNOWLEDGMENTS

The authors would like to thank the Deutsche Forschungsgemeinschaft (DFG) (SFB595 "Electrical Fatigue of functional materials," SPP1181 "Nanomat," Grant No. JA859/12-1), the Bundesministerium für Bildung und Forschung (BMBF) (Grant No. 05ES3XBA/5), the BMBF Verbundprojekt LISA under Grant No. 03SF0327D and the European Union (Network of Excellence "FAME" and FP5 RTN INTERCALNET) for financial support. Ralf Hunger from TU Darmstadt, Patrick Hoffmann and Dieter Schmeisser from BTU Cottbus, Christian Pettenkofer from HMI Berlin, and the BESSY staff are acknowledged for supporting the synchrotron beamtimes. The Jülich Supercomputing Centre has supported the calculations.

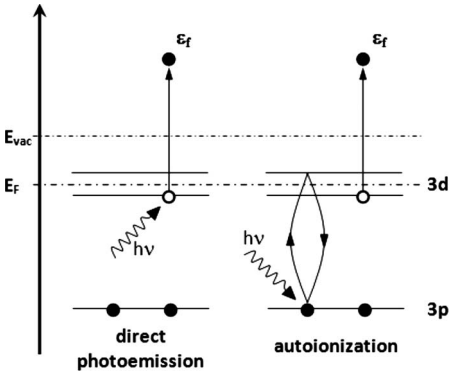

FIG. 21. Illustration of photoionization processes: (a) direct photoemission and (b) autoionization.

APPENDIX: A SHORT SURVEY OF PES EFFECTS IN $LiCoO_2$

A brief overview of the theory of ResPES will be given, in particular, using the example of $LiCoO_2$. For more detailed information about this technique refer to related publications of resonant photoemission theory[94–98] and experiments.[67,88,89,99–106]

1. Photoemission final states

a. Direct photoemission

For $LiCoO_2$ a direct photoemission process from a Co $3d$ level can be represented in the atomic orbital notation as follows:

$$E(\text{Co } 3p^6 3d^6) + h\nu \rightarrow E(\text{Co } 3p^6 3d^5) + \varepsilon_f. \quad (3)$$

In this case the resulting final state is described by a Co $3p^6 3d^5$ electron configuration with a photoionization hole in cobalt-derived t_{2g} states and ε_f represents the emitted photoelectron [Fig. 21(a)].

By removing an electron from $3d$ valence states the energy of the remaining electrons is altered. A larger effective core potential leads to a stronger Coulomb interaction with the remaining $3d$ electrons whereas the valence-band states of the ligands (the oxygen $2p$-like states) will be affected to a much lesser extent. As a result, the binding energy of cobalt-derived valence-band states will be increased relatively to those of the ligands hence direct photoemission processes will be observed at higher binding energies.[85,107] In the case of lithiated transition-metal oxides such as $LiCoO_2$

the possibility of a L-M charge transfer has to also be taken into account, as a notable covalent mixing of cobalt and oxygen states can be found.[17,24]

b. Charge-transfer final state

Due to the photoemission of a Co 3*d* electron, remaining electrons are bonded more strongly and the energy of those states can *drop* below the energy of the ligand band onset. For a sufficient overlap between oxygen- and cobalt-derived states, i.e., a strong covalency of the bond,[17,24] an L-M charge transfer can occur, filling the 3*d* hole state. The photoinduced hole at the Co ion is transferred to oxygen ligands and by this forming a charge-transfer state (where *L* denotes a hole in the ligand band)

$$E(\mathrm{Co}\ 3p^6 3d^6) + h\nu \rightarrow E(\mathrm{Co}\ 3p^6 3d^6 L) + \varepsilon_\mathrm{f}. \quad (4)$$

As a consequence of this charge transfer, states with dominant Co-like character are more efficiently shielded and are less affected by the additional core hole. Charge-transfer states are therefore in their final-state energy mostly unaffected by the photoemission process. In contrary to direct photoemission, a *screened* final state is observed, which can be close to the ground state of the system (dependent on the extent of screening).

The relative intensities of both final state contributions depend primarily on the probability of an L-M charge transfer. In ionic solids the direct photoemission is dominant. In covalent solids a charge transfer becomes more likely and hence the probability for a charge-transfer final state (Co $3p^6 3d^6 L$) increases. According to Jeng *et al.*[108] this is also valid for photoemission from nonbonding (atomic) orbitals in covalent solids. In case of $LiCoO_2$ both photoemission processes contribute to the final state due to the covalent bonding contribution in the Co-O bond.

c. Autoionization

The direct photoemission process [Eq. (2)], which can also lead to a charge-transfer final state [Eq. (3)], is nonresonant and occurs at all photon energies large enough, to excite an electron above the vacuum level (E_vac). However, if the excitation energy is varied close to the Co 3*p* core-level binding energy and exceeds the threshold energy for a Co 3*p*-3*d* transition, which is about 62 eV for $LiCoO_2$, the probability for an alternative excitation process increases. By x-ray absorption a 3*p* electron can be excited into empty 3*d* orbitals, resulting in an excited state

$$E(\mathrm{Co}\ 3p^6 3d^6) + h\nu \rightarrow E([\mathrm{Co}\ 3p^5 3d^7]^*). \quad (5)$$

A decay channel for the excited $3p^5 3d^{n+1}$ state is a super-Coster-Kronig process according to Davis *et al.*,[97,109] which results in an emitted photoelectron

$$E([\mathrm{Co}\ 3p^5 3d^7]^*) \rightarrow E(\mathrm{Co}\ 3p^6 3d^5) + \varepsilon_\mathrm{f}. \quad (6)$$

This process is referred to as autoionization, see Fig. 21(b).

Initial and final states of the autoionization [Eq. (4) and (5)] are similar to the direct photoemission [Eq. (2)]. Also the kinetic energy of the emitted photoelectron is identical in both cases and depends on the excitation energy:[85] $E_{kin}^{auto} = E(\mathrm{Co}\ 3p^5 3d^{7*}) - h\nu - E(\mathrm{Co}\ 3p^6 3d^5) = E_{kin}^{direct}$. Thus, both processes are coherent, which allows an interference and by this a resonant modulation of the photoionization cross section.

Likewise to the direct photoemission, a charge-transfer process can be assumed *after* the autoionization, resulting in a Co $3p^6 3d^6 L$ final-state configuration, which, in principle, can interfere with a charge-transfer transition [Eq. (3)]. According to Kemp *et al.*[26] also a notable admixture of a $d^{n+1}L$ configuration has to be considered for the ground state of $LiCoO_2$, assuming a negative value of the charge-transfer gap ($\Delta = -0.5$ eV). Van Elp *et al.*[24] estimated a ground-state configuration of 47% d^6, 44% $d^7 L$, and 9% $d^8 L^2$. As a consequence, additional possibilities of interfering transitions have to be considered, e.g.,

$$E(\mathrm{Co}\ 3p^6 3d^7 L) + h\nu \rightarrow E([\mathrm{Co}\ 3p^5 3d^8 L]^*), \quad (7)$$

$$E([\mathrm{Co}\ 3p^5 3d^8 L]^*) \rightarrow E(\mathrm{Co}\ 3p^6 3d^6 L) + \varepsilon_\mathrm{f}. \quad (8)$$

This autoionization process is in turn coherent to direct photoemission from a charge-transfer ground state.

The characteristic devolution of such a resonance has been described theoretically by Fano.[110] The theory treats the interaction of discrete states (Co $3p^5 3d^{n+1}$) with continuum states (Co $3p^6 3d^{n-1}\varepsilon_\mathrm{f}$) of the same energy E_0 during autoionization. The resulting modulation of the photoionization cross section close to the resonance energy is described by a Fano profile (Fig. 7)

$$\sigma(E) \propto \frac{(q+\varepsilon)^2}{1+\varepsilon^2} \quad \text{with} \quad \varepsilon = \frac{E - E_0}{\Gamma}. \quad (9)$$

The intensity of the interference (resonance) depends on the energy difference between photons and the threshold energy ($E - E_0$). The asymmetry parameter q contains the phase correlation between the interfering transitions and defines the energy dependence of the resonance profile. The relative energy $E - E_0$ is normalized by parameter Γ, which describes the FWHM of the resonance and includes instrumental broadening.

*Corresponding author; david.ensling@gmail.com

[1] G. G. Amatucci, J. M. Tarascon, and L. C. Klein, J. Electrochem. Soc. **143**, 1114 (1996).

[2] H. Benqlilou-Moudden, G. Blondiaux, P. Vinatier, and A. Levasseur, Thin Solid Films **333**, 16 (1998).

[3] G. Chen, W. Hao, Y. Shi, and Y. Wu, J. Mater. Res. **15**, 583 (2000).

[4] R. Dedryvère, H. Martinez, S. Leroy, D. Lemordant, F. Bonhomme, P. Biensan, and D. Gonbeau, J. Power Sources **174**, 462 (2007).

[5] M. Hirayama, N. Sonoyama, T. Abe, M. Minoura, M. Ito, D. Mori, A. Yamada, R. Kanno, T. Terashima, M. Takano, K. Tamura, and J. Mizuki, J. Power Sources **168**, 493 (2007).
[6] Z. G. Li, R. L. Harlow, F. Gao, P. Lin, R. Miao, and L. Liang, J. Electrochem. Soc. **150**, A1171 (2003).
[7] V. Kalai Vani and O. M. Hussain, Ionics **13**, 473 (2007).
[8] B. Wang, J. B. Bates, F. X. Hart, B. C. Sales, R. A. Zuhr, and J. D. Robertson, J. Electrochem. Soc. **143**, 3203 (1996).
[9] H. F. Wang, Y. I. Jang, B. Y. Huang, D. R. Sadoway, and Y. T. Chiang, J. Electrochem. Soc. **146**, 473 (1999).
[10] J. C. Dupin, D. Gonbeau, H. Benqlilou-Moudden, P. Vinatier, and A. Levasseur, Thin Solid Films **384**, 23 (2001).
[11] D. Ensling, A. Thissen, Y. Gassenbauer, A. Klein, and W. Jaegermann, Adv. Eng. Mater. **7**, 945 (2005).
[12] K. Nakamura, M. Yamamoto, K. Okamura, Y. Michihiro, I. Nakabayashi, and T. Kanashiro, Solid State Ionics **121**, 301 (1999).
[13] W. S. Yoon, K. K. Lee, and K. B. Kim, J. Electrochem. Soc. **147**, 2023 (2000).
[14] W. D. Johnston, R. R. Heikes, and D. Sestrich, J. Phys. Chem. Solids **7**, 1 (1958).
[15] M. T. Czyżyk, R. Potze, and G. A. Sawatzky, Phys. Rev. B **46**, 3729 (1992).
[16] J. van Elp, R. H. Potze, H. Eskes, R. Berger, and G. A. Sawatzky, Phys. Rev. B **44**, 1530 (1991).
[17] V. R. Galakhov, E. Z. Kurmaev, S. Uhlenbrock, M. Neumann, D. G. Kellerman, and V. S. Gorshkov, Solid State Commun. **99**, 221 (1996).
[18] L. Y. Hu, Z. H. Xiong, C. Y. Ouyang, S. Q. Shi, Y. H. Ji, M. S. Lei, Z. X. Wang, H. Li, X. J. Huang, and L. Q. Chen, Phys. Rev. B **71**, 125433 (2005).
[19] F. Huang, H. Zhan, and Y. H. Zhou, Chin. J. Chem. **21**, 1275 (2003).
[20] F. M. F. de Groot, M. Abbate, J. Vanelp, G. A. Sawatzky, Y. J. Ma, C. T. Chen, and F. Sette, J. Phys.: Condens. Matter **5**, 2277 (1993).
[21] C. A. Marianetti, G. Kotliar, and G. Ceder, Nature Mater. **3**, 627 (2004).
[22] L. A. Montoro, M. Abbate, E. C. Almeida, and J. M. Rosolen, Chem. Phys. Lett. **309**, 14 (1999).
[23] L. A. Montoro, M. Abbate, and J. M. Rosolen, Electrochem. Solid-State Lett. **3**, 410 (2000).
[24] J. van Elp, J. L. Wieland, H. Eskes, P. Kuiper, G. A. Sawatzky, F. M. F. de Groot, and T. S. Turner, Phys. Rev. B **44**, 6090 (1991).
[25] J. van Elp and A. Tanaka, Phys. Rev. B **60**, 5331 (1999).
[26] J. P. Kemp and P. A. Cox, J. Phys.: Condens. Matter **2**, 9653 (1990).
[27] D. Ensling, F. Fernandez-Madrigal, A. Thissen, and W. Jaegermann, in *203rd ECS Meeting*, edited by K. Zaghib, C. M. Julien, and J. Prakash (Proc. ECS, Paris, 2003), p. 585.
[28] V. R. Galakhov, V. V. Karelina, D. G. Kellerman, V. S. Gorshkov, N. A. Ovechkina, and M. Neumann, Phys. Solid State **44**, 266 (2002).
[29] V. R. Galakhov, E. Z. Kurmaev, S. Uhlenbrock, M. Neumann, D. G. Kellerman, and V. S. Gorshkov, Solid State Commun. **95**, 347 (1995).
[30] V. R. Galakhov, N. A. Ovechkina, A. S. Shkvarin, S. N. Shamin, E. Z. Kurmaev, K. Kuepper, A. F. Takacs, M. Raekers, S. Robin, M. Neumann, G. N. Gavrila, A. S. Semenova, D. G. Kellerman, T. Kaambre, and J. Nordgren, Phys. Rev. B **74**, 045120 (2006).
[31] J. Graetz, A. Hightower, C. C. Ahn, R. Yazami, P. Rez, and B. Fultz, J. Phys. Chem. B **106**, 1286 (2002).
[32] M. G. Kim, H. J. Shin, J. H. Kim, S. H. Park, and Y. K. Sun, J. Electrochem. Soc. **152**, A1320 (2005).
[33] Y. Koyama, T. Mizoguchi, H. Ikeno, and I. Tanaka, J. Phys. Chem. B **109**, 10749 (2005).
[34] P. Y. Liao, J. G. Duh, and H. S. Sheu, Electrochem. Solid-State Lett. **10**, A88 (2007).
[35] A. W. Moses, H. G. G. Flores, J. G. Kim, and M. A. Langell, Appl. Surf. Sci. **253**, 4782 (2007).
[36] T. Ohzuku and Y. Makimura, Res. Chem. Intermed. **32**, 507 (2006).
[37] W. S. Yoon, M. Balasubramanian, X. Q. Yang, Z. G. Fu, D. A. Fischer, and J. McBreen, J. Electrochem. Soc. **151**, A246 (2004).
[38] W. S. Yoon, K. Y. Chung, J. McBreen, D. A. Fischer, and X. Q. Yang, J. Power Sources **163**, 234 (2006).
[39] S. Laubach, S. Laubach, P. C. Schmidt, D. Ensling, S. Schmid, W. Jaegermann, A. Thissen, K. Nikolowski, and H. Ehrenberg, Phys. Chem. Chem. Phys. **11**, 3278 (2009).
[40] K. Kushida and K. Kuriyama, Solid State Commun. **129**, 525 (2004).
[41] H. Tukamoto and A. R. West, J. Electrochem. Soc. **144**, 3164 (1997).
[42] J. Wolfenstine, J. Power Sources **129**, 324 (2004).
[43] P. Ghosh, S. Mahanty, M. W. Raja, R. N. Basu, and H. S. Maiti, J. Mater. Res. **22**, 1162 (2007).
[44] K. Kushida and K. Kuriyama, Solid State Commun. **123**, 349 (2002).
[45] J. M. Rosolen, J. Electroanal. Chem. **501**, 253 (2001).
[46] W. S. Yoon, K. B. Kim, M. G. Kim, M. K. Lee, H. J. Shin, J. M. Lee, J. S. Lee, and C. H. Yo, J. Phys. Chem. B **106**, 2526 (2002).
[47] C. H. Chen, B. J. Hwang, C. Y. Chen, S. K. Hu, J. M. Chen, H. S. Sheu, and J. F. Lee, J. Power Sources **174**, 938 (2007).
[48] D. Ensling, A. Thissen, and W. Jaegermann, Appl. Surf. Sci. **255**, 2517 (2008).
[49] F. M. Alamgir, E. Strauss, M. denBoer, S. Greenbaum, J. F. Whitacre, C.-C. Kao, and S. Neih, J. Electrochem. Soc. **152**, A845 (2005).
[50] J. B. Bates, N. J. Dudney, B. J. Neudecker, F. X. Hart, H. P. Jun, and S. A. Hackney, J. Electrochem. Soc. **147**, 59 (2000).
[51] P. J. Bouwman, B. A. Boukamp, H. J. M. Bouwmeester, and P. H. L. Notten, Solid State Ionics **152-153**, 181 (2002).
[52] G. A. Wei, T. E. Haas, and R. B. Goldner, Solid State Ionics **58**, 115 (1992).
[53] J. B. Bates, N. J. Dudney, B. Neudecker, A. Ueda, and C. D. Evans, Solid State Ionics **135**, 33 (2000).
[54] S. I. Cho and S. G. Yoon, Appl. Phys. Lett. **82**, 3345 (2003).
[55] W. G. Choi and S. G. Yoon, J. Power Sources **125**, 236 (2004).
[56] C. N. P. da Fonseca, J. Davalos, M. Kleinke, M. C. A. Fantini, and A. Gorenstein, J. Power Sources **81-82**, 575 (1999).
[57] N. J. Dudney and Y. I. Jang, J. Power Sources **119-121**, 300 (2003).
[58] P. Fragnaud, T. Brousse, and D. M. Schleich, J. Power Sources **63**, 187 (1996).
[59] H. Y. Park, S. C. Nam, Y. C. Lim, K. G. Choi, K. C. Lee, G. B. Park, J. B. Kim, H. P. Kim, and S. B. Cho, Electrochim. Acta **52**, 2062 (2007).
[60] J. F. Whitacre, W. C. West, E. Brandon, and B. V. Ratnakumar, J. Electrochem. Soc. **148**, A1078 (2001).

[61] C. L. Liao and K. Z. Fung, J. Power Sources **128**, 263 (2004).
[62] J. J. Yeh and I. Lindau, At. Data Nucl. Data Tables **32**, 1 (1985).
[63] T. Bredow and A. R. Gerson, Phys. Rev. B **61**, 5194 (2000).
[64] O. Bengone, M. Alouani, P. Blochl, and J. Hugel, Phys. Rev. B **62**, 16392 (2000).
[65] T. Mayer, M. Lebedev, R. Hunger, and W. Jaegermann, Appl. Surf. Sci. **252**, 31 (2005).
[66] SPECS GmbH, Manual of PHOIBOS HCA3500, Berlin (2003).
[67] S. Laubach, P. C. Schmidt, A. Thissen, F. J. Fernandez-Madrigal, Q. H. Wu, W. Jaegermann, M. Klemm, and S. Horn, Phys. Chem. Chem. Phys. **9**, 2564 (2007).
[68] H. Ikeno, F. M. F. de Groot, E. Stavitski, and I. Tanaka, J. Phys.: Condens. Matter **21** 104208 (2009).
[69] F. de Groot, Coord. Chem. Rev. **249**, 31 (2005).
[70] V. R. S. R. Dovesi, C. Roetti, R. Orlando, C. M. Zicovich-Wilson, F. Pascale, B. Civalleri, K. Doll, N. M. Harrison, I. J. Bush, P. D'Arco, M. Llunell, (University of Torino, University of Torino, 2006).
[71] J. C. Slater and G. F. Koster, Phys. Rev. **94**, 1498 (1954).
[72] G. Kresse and J. Hafner, Phys. Rev. B **48**, 13115 (1993).
[73] G. Kresse and J. Hafner, Phys. Rev. B **49**, 14251 (1994).
[74] G. Kresse, Comput. Mater. Sci. **6**, 15 (1996).
[75] G. Kresse and J. Furthmuller, Phys. Rev. B **54**, 11169 (1996).
[76] G. Kresse and D. Joubert, Phys. Rev. B **59**, 1758 (1999).
[77] J. P. Perdew, K. Burke, and M. Ernzerhof, Phys. Rev. Lett. **77**, 3865 (1996).
[78] S. L. Dudarev, G. A. Botton, S. Y. Savrasov, C. J. Humphreys, and A. P. Sutton, Phys. Rev. B **57**, 1505 (1998).
[79] A. D. Becke, J. Chem. Phys. **98**, 1372 (1993).
[80] T. Bredow, Phys. Rev. B **70**, 115111 (2004).
[81] F. F. F. R. Dovesi, C. Roetti, and V. R. Saunders, Faraday Discuss. **106**, 173 (1997).
[82] T. Bredow, K. Jug, and R. A. Evarestov, Phys. Status Solidi B **243**, R10 (2006).
[83] T. Ohzuku and A. Ueda, J. Electrochem. Soc. **141**, 2972 (1994).
[84] E. Rossen, J. N. Reimers, and J. R. Dahn, Solid State Ionics **62**, 53 (1993).
[85] S. Hufner, *Photoelectron Spectroscopy* (Springer, New York, 1995).
[86] A. P. C. C. J. Bradley, *The Mathematical Theory of Symmetry in Solids: Representations Theory for Point Groups and Space Group* (Clarendon Press, Oxford, 1972).
[87] E. A. Mikajlo, K. L. Nixon, V. A. Coleman, and M. J. Ford, J. Phys.: Condens. Matter **14**, 3587 (2002).
[88] S. P. Jeng, Z. M. Zhang, and V. E. Henrich, Phys. Rev. B **44**, 3266 (1991).
[89] H. W. Nesbitt, I. Uhlig, G. M. Bancroft, and R. Szargan, Am. Mineral. **88**, 1279 (2003).
[90] M. P. Seah and W. A. Dench, Surf. Interface Anal. **1**, 2 (1979).
[91] F. M. F. de Groot, M. Grioni, J. C. Fuggle, J. Ghijsen, G. A. Sawatzky, and H. Petersen, Phys. Rev. B **40**, 5715 (1989).
[92] A. E. Bocquet, T. Mizokawa, T. Saitoh, H. Namatame, and A. Fujimori, Phys. Rev. B **46**, 3771 (1992).
[93] J. Zaanen, G. A. Sawatzky, and J. W. Allen, J. Magn. Magn. Mater. **54-57**, 607 (1986).
[94] A. Tanaka and T. Jo, J. Phys. Soc. Jpn. **63**, 2788 (1994).
[95] L. C. Davis and L. A. Feldkamp, Phys. Rev. Lett. **44**, 673 (1980).
[96] A. Zangwill and P. Soven, Phys. Rev. Lett. **45**, 204 (1980).
[97] L. C. Davis and L. A. Feldkamp, Phys. Rev. B **23**, 6239 (1981).
[98] L. C. Davis, Phys. Rev. B **25**, 2912 (1982).
[99] E. Bertel, R. Stockbauer, R. L. Kurtz, D. E. Ramaker, and T. E. Madey, Phys. Rev. B **31**, 5580 (1985).
[100] Z. M. Zhang, S. P. Jeng, and V. E. Henrich, Phys. Rev. B **43**, 12004 (1991).
[101] C. Guillot, Y. Ballu, J. Paigne, J. Lecante, K. P. Jain, P. Thiry, R. Pinchaux, Y. Petroff, and L. M. Falicov, Phys. Rev. Lett. **39**, 1632 (1977).
[102] J. W. Allen, S. J. Oh, I. Lindau, J. M. Lawrence, L. I. Johansson, and S. B. Hagstrom, Phys. Rev. Lett. **46**, 1100 (1981).
[103] M. R. Thuler, R. L. Benbow, and Z. Hurych, Phys. Rev. B **26**, 669 (1982).
[104] T. Takahashi, H. Matsuyama, H. Katayamayoshida, Y. Okabe, S. Hosoya, K. Seki, H. Fujimoto, M. Sato, and H. Inokuchi, Nature (London) **334**, 691 (1988).
[105] J. W. Allen, C. G. Olson, M. B. Maple, J. S. Kang, L. Z. Liu, J. H. Park, R. O. Anderson, W. P. Ellis, J. T. Markert, Y. Dalichaouch, and R. Liu, Phys. Rev. Lett. **64**, 595 (1990).
[106] Q. H. Wu, A. Thissen, W. Jaegermann, M. Schuz, and P. C. Schmidt, Chem. Phys. Lett. **430**, 309 (2006).
[107] G. van der Laan, C. Westra, C. Haas, and G. A. Sawatzky, Phys. Rev. B **23**, 4369 (1981).
[108] S. P. Jeng and V. E. Henrich, Solid State Commun. **75**, 1013 (1990).
[109] L. C. Davis, J. Appl. Phys. **59**, R25 (1986).
[110] U. Fano, Phys. Rev. **124**, 1866 (1961).